Copyright Warning & Restrictions

The copyright law of the United States (Title 17, United States Code) governs the making of photocopies or other reproductions of copyrighted material.

Under certain conditions specified in the law, libraries and archives are authorized to furnish a photocopy or other reproduction. One of these specified conditions is that the photocopy or reproduction is not to be "used for any purpose other than private study, scholarship, or research." If a, user makes a request for, or later uses, a photocopy or reproduction for purposes in excess of "fair use" that user may be liable for copyright infringement,

This institution reserves the right to refuse to accept a copying order if, in its judgment, fulfillment of the order would involve violation of copyright law.

Please Note: The author retains the copyright while the New Jersey Institute of Technology reserves the right to distribute this thesis or dissertation

Printing note: If you do not wish to print this page, then select "Pages from: first page # to: last page #" on the print dialog screen

ABSTRACT

CHARACTERIZATION OF STEEL CORROSION IN AN AGGRESSIVE ENVIRONMENT

by
Sung Min Maeng

As part of the Sustainable Green Manufacturing Program, the corrosion resistance of sputtered tantalum is being studied in order to evaluate it as a replacement coating for electroplated chrome. To accomplish this, studies were conducted to evaluate corrosion properties of the gun barrel steel by employing corrosion rate and bulk measurements including x-ray diffraction (XRD), scanning electron microscopy (SEM)/energy dispersive x-ray spectroscopy (EDX), and x-ray fluorescence (XRF), as well as synchrotron-based x-ray absorption spectroscopy (XAS).

Corrosion behavior of steel immersed in an aggressive environment of 37.8 % hydrochloric acid at room temperature was investigated as a function of time from 10 minutes to 41 hours. The corrosion rate peaked between 1 and 8 hours of exposure, and revealed a gradual decrease as exposure time increased. SEM/EDX analysis showed that the surface of corroded steel was attacked differently as a function of time, but time had no significant effect on the composition of corrosion product. During the tests, defects on the surface of the polished steel resulted in pitting corrosion. With XRF the bulk composition of the corroded products was found to be consistent with the surface analysis using EDX. XRD analyses of this corrosion product on the surfaces indicated the formation of β-FeOOH (akaganeite) and possibly minor amounts of other oxides. In XAS analysis, the spectra revealed that iron has different coordination environments in steel and the oxide. However, iron in all the corroded specimens appears to have oxygen as the first neighbor. This study provides a baseline for future corrosion research and an exploration of characterization methods for the corroded surface.

CHARACTERIZATION OF STEEL CORROSION IN AN AGGRESSIVE ENVIRONMENT

by
Sung Min Maeng

A Thesis
Submitted to the Faculty of
New Jersey Institute of Technology
In Partial Fulfillment of the Requirements for the Degree of
Master of Science in Environmental Engineering

Department of Civil and Environmental Engineering

August 1999

APPROVAL PAGE

CHARACTERIZATION OF STEEL CORROSION IN AN AGGRESSIVE ENVIRONMENT

Sung Min Maeng

Dr. Lisa B. Axe, Thesis Advisor — Date
Assistant Professor of Civil and Environmental Engineering, NJIT

Dr. Hsin-Neng Hsieh, Committee Member — Date
Professor and Associate Chair of Civil and Environmental Engineering, NJIT

Dr. Daniel J. Watts, Committee Member — Date
Deputy Executive Director of Center for Environmental Engineering and Science, NJIT

Dr. Trevor A. Tyson, Committee Member — Date
Assistant Professor of Physics, NJIT

BIOGRAPHICAL SKETCH

Author: Sung Min Maeng

Degree: Master of Science in Environmental Engineering

Date: August 1999

Undergraduate and Graduate Education:

- Master of Science in Environmental Engineering,
  New Jersey Institute of Technology, Newark, NJ, 1999
- Master of Science in Environmental Engineering,
  Inha University, Incheon, Korea, 1996
- Bachelor of Science in Environmental Engineering,
  Inha University, Incheon, Korea, 1994

Major: Environmental Engineering

This thesis is dedicated to
my parents and my wife

ACKNOWLEDGMENT

I wish to express my sincere appreciation to my advisor Dr. Lisa Axe for her invaluable guidance, enthusiastic encouragement, and precious advice through this research. I also wish to thank Dr. Trevor Tyson for his valuable comment and advice through this research.

I am greatly thankful to Dr. Daniel Watts and Dr. Hsin-Neng Hsieh for their effort and valuable comment as members of the committee. I am grateful to Dr. Marek Sosnowski for providing gun-barrel steel samples for this research, and thank to Mr. Chandrakant Patel for his technical help and comment.

I appreciate the friendship and encouragement from Paras Trivedi and Hiran Upadhya. And finally, a special thank to my wife, Jeeyoung Park, for her love, encouragement, and patience.

TABLE OF CONTENTS

Chapter **Page**

TABLE OF CONTENTS
(Continued)

Chapter **Page**

LIST OF TABLES

Table **Page**

LIST OF FIGURES

Figure **Page**

CHAPTER 1

INTRODUCTION

1.1 Corrosion and Protection

Metals or alloys used in the environment can deteriorate and can be released to some extent through corrosion processes. Corrosion is considered to be the largest single cause of plant or equipment breakdown. In the U.S., costs currently exceed $300 billion per year to replace corroded materials [1]. Moreover, components released from corrosion may be toxic to our environment. These economical and environmental problems caused by corrosion force us to develop corrosion protection methods.

Often, corrosion resistant thin coatings are used for the protection of metal substrates. These relatively thin coatings can play a role as a stable barrier between the metal substrate and its environment. Chromium has been used extensively as a constituent of many alloys as well as a coating on other metals because of its high corrosion resistance and hardness [2]. Chromium is typically electroplated from its hexavalent form. Environmentally, however, hexavalent chromium, is not only a known carcinogen and thus toxic to handle, but also the treatment of wastes generated from electroplating process is costly [3].

Tantalum metal is being investigated as a protective material for severe corrosive environments such as those exhibited in gun-barrels, because of its refractory and ductile properties as well as its highly corrosion resistant nature. Tantalum pentoxide, which forms a very thin outer film, is a protective coating with outstanding corrosion resistance and inertness properties as well [4]. In terms of toxicology, the effect of tantalum in the environment is currently under investigation, but it is expected to be much less of a

potential threat [5] than chromium. Therefore, the purpose of this research is to investigate the effect of replacing electroplated chrome with sputtered tantalum in protecting steel substrates from corrosion thereby reducing a potential threat to the environment.

Corrosion is defined as destruction or deterioration of a material, usually mass loss of metal or alloy due to interaction between a material and its surrounding environment. Corrosion behavior is explained as a combined property of a material and its environment to which it is exposed as well as the property of the resulting corrosion product. The corrosion rate or resistance of a metal are affected by a number of processes including reduction-oxidation (redox), reaction kinetics (e.g., oxide precipitation and dissolution), and mass transfer. Because of the combination of these processes, it is often difficult to distinguish between them and elicit the rate-limiting mechanism.

The most stable configuration of a metal is an arrangement in which the atoms of a metal are coordinated in a regular, ordered way. Since the grain boundaries, the disordered region in a metal, are of higher energy and more active chemically than the lattice structure, grain boundaries are usually attacked more rapidly than the ordered structure (lattice) when exposed to a corrosive environment [6].

All metals and alloys have a tendency to revert to their most thermodynamically stable form. As a result, some of the elements of the metal or alloy change from a metallic state into a nonmetallic state (metal oxides). The energy of the corrosion system is lowered as the metal is converted to a lower-energy form. The change in the Gibbs free energy (ΔG) between a metal state and its oxide form is the driving force for the corrosion process. Through thermodynamics, the tendency for corrosion and its process to occur can be examined and quantified, and the composition of the corrosion product

can be predicted. Corroding systems are not in equilibrium [6], and therefore the understanding, modeling, and predicting kinetics or rates of corrosion is most important.

Corrosion is a reaction involving oxidation and reduction. In electrochemical terms, a metal is oxidized to produce metal ions and electrons (anodic reaction). For example, the reaction of $Fe \rightarrow Fe^{2+} + 2e^-$ has a standard potential (E^o) of 0.44 Volt. Subsequently, the metal ions precipitate into such forms as oxides (corrosion products) which are often very stable in the corrosive environment. Cathodic (reduction) reactions consume electrons and yield various products, according to the nature of the environment. For example, some cathodic reactions that may occur at the steel surface include

$$\text{Hydrogen evolution:} \quad 2H^+ + 2e^- \rightarrow H_2, \; E^o = 0 \text{ (V) or}$$

$$\text{Acidic Oxygen reduction:} \quad O_2 + 4H^+ + 4e^- \rightarrow 2H_2O, \; E^o = 1.229 \text{ (V) or}$$

$$\text{Alkaline Oxygen reduction:} \quad O_2 + 2H_2O + 4e^- \rightarrow 4OH^-, \; E^o = 0.401 \text{ (V)}$$

When iron corrosion (metal oxidation) occurs in an acid solution, hydrogen evolution or acidic oxygen reduction occurs to maintain electronic neutrality. The standard redox potentials associated with hydrogen evolution or acidic oxygen reduction are 0.44 (V) and 1.67 (V), respectively. A positive standard redox potential indicates the corrosion process is spontaneous.

Anodic reactions occur simultaneously with cathodic reactions. The overall process may be controlled by one of several reactions, including the anodic or cathodic reactions listed above. Moreover, the corrosion rate may be controlled by mass transport of the oxidizing agent in electrolyte or through the corrosion product between the metal and bulk solution. The corrosion product may inhibit the mass transfer flux of the oxidizing agent to the surface due to porosity and tortuosity of the corrosion product. This film then acts as barrier between the corrosion site and its corrosive environment. Corrosion

control is possible by eliminating either the anodic or the cathodic process, or by eliminating the corrosion-promoting aspects of the environment [7].

With respect to corrosion protection, the objectives of this research are to develop methods to characterize the corrosion process in an effort to better understand the associated mechanisms. Subsequently, corrosion models for steel as well as tantalum will be employed for aggressive environments such as high temperature and pressure.

Before performing the corrosion studies on tantalum, corrosion tests on the steel substrate were conducted as a function of time in concentrated hydrochloric acid, the most chemically corrosive medium for steel. In addition to the corrosion tests, the following analytical methods were employed to evaluate the properties of the corrosion process in detail:

- Corrosion rate was measured using weight loss measurement.
- Crystallographic examination of the steel substrate and its corroded specimens was performed with x-ray diffraction, and the structural information was used to identify the corrosion products.
- Scanning electron microscopy was used to obtain the morphological images of the steel substrate and its corrosion products. Quantitative elemental composition of corrosion products on the corroded specimens was assessed with energy dispersive x-ray spectroscopy.
- Local structural information at the atomic scale was acquired using x-ray absorption spectroscopy.

CHAPTER 2

LITERATURE FOR CHARACTERIZATION METHODS OF CORROSION

In this section, a literature review is presented of methods used to study corrosion and the resulting products. These methods include the mass loss measurement, visual evaluation, metal ion measurement, electrochemical impedance spectroscopy, x-ray diffraction, x-ray fluorescence, scanning electron microscopy/energy dispersive x-ray spectroscopy, and x-ray absorption fine structure spectroscopy.

2.1 Mass Loss Measurement

Corrosion damage is generally assessed quantitatively by mass loss measurement [8]. Corrosion rate is represented as loss of metal thickness as a function of time. However, corrosion rates can be expressed as mass gain rather than mass loss in cases where the corrosion products are so tightly bound on the surface of the metal specimen that they cannot be removed by ordinary chemical and mechanical means.

Mass loss measurement of corrosion is valid only in the case of uniform corrosion because corrosion rates from mass loss measurement may be misleading when pitting or crevice corrosion occurs. Mass loss represents the difference between the mass of sample before and after the corrosion test. Subsequent to the corrosion test, the corrosion product should be carefully removed from the surface of the sample because any corrosion product, which is weighed, may result in an incorrect measurement.

Using this method, the corrosion rate is determined by the measured loss in weight per unit area per time. The equation for calculating the corrosion rate is as follows

$$Corrosion\ \ rate = \frac{K \times W}{D \times A \times t}$$

where K is a conversion factor (Table 2.1), W is the mass loss in grams, D is the density of metal specimen in g/cm^3, A is the exposed area of metal specimen in cm^2, and t is the exposure time in hours.

Table 2.1 Conversion factor (K) for corrosion rate units [8].

Corrosion rate units	Constant (k)
mils per year (mpy)	3.45×10^6
inches per year (ipy)	3.45×10^3
inches per month (ipm)	2.87×10^2
millimeters per year (mm/yr)	8.76×10^4
micrometers per year (μm/yr)	8.76×10^7
grams per square meter per hour ($g/m^2 \cdot h$)	$1.00\times10^4\times D$
milligrams per square decimeter per day (mdd)	$2.40\times10^6\times D$
micrograms per square meter per second ($\mu g/m^2 \cdot s$)	$2.78\times10^6\times D$

Because the assessment of corrosion damage by mass loss measurement is based on the mode of uniform corrosion, it is necessary to evaluate the corrosion mode such as pitting, crevice, or cracking through visual evaluation.

2.2 Visual Evaluation

Visual observation with or without a magnifying lens is a simple way to examine corrosion damage and the corrosion experiment [9]. Initial observation in any corrosion test includes visual evaluation, which can provide information on corrosion type and the color of the corrosion product; documentation is accomplished easily with a photograph.

Corrosion modes as well as the correlation between corrosion mode and microstructure can be evaluated with optical microscopy.

2.3 Metal Ion Measurement in Solution

The concentration of the metal in solution provides the additional information for mass loss measurement [10]. In the case of the immersion corrosion test, instrumentation such as atomic absorption (AA) spectroscopy or inductively coupled plasma spectroscopy (ICP) provides rapid analysis of the metal as corrosion occurs. The amount of metal associated with the corrosion product can be calculated by subtracting the amount of dissolved metal from the mass loss measurement.

2.4 Electrochemical Impedance Spectroscopy (EIS)

As mentioned in Chapter 1, corrosion is a process involving oxidation and reduction reactions between the metal surface and its environment. Through this redox reaction, an electrochemical potential called the corrosion potential is produced. A more accurate measurement of the corrosion rate can be acquired through an electrochemical analysis as opposed to the mass loss measurement.

Electrochemical impedance spectroscopy (EIS) is one of the most advanced methods in studying the electrochemical system. The corrosion rate of a metal can be measured without the complications of the polarization and associated resistance methods [11]. There are two techniques widely used in EIS [12]. One is the called the single-sine technique that applies a single frequency signal to an electrochemical cell and measures the response. The other is called the multi-sine technique, and is more suitable for a corroding system. Once raw data consisting of voltage and current components with real

and imaginary parts are acquired, several output formats can be plotted with this data. These output formats include, but are not limited to, the Nyquist, Bode, and Randles plots, which provide corrosion characteristics in the electrochemical reaction.

The concept of polarization is of importance in understanding corrosion behavior and corrosion reactions from the electrochemical vantage [6]. Polarization can be divided into activation polarization and concentration polarization. Activation polarization refers to an electrochemical process that is controlled by the reaction sequence at the metal-electrolyte interface. Concentration polarization refers to electrochemical reactions that are controlled by diffusion of the species from the electrolyte to the electrode surface.

The Tafel plot plays an important role in measurement of the corrosion current (i_{corr}), which is used in calculating corrosion rate. The corrosion current can be obtained directly from a Tafel plot or can be calculated from the Tafel constants (β_A and β_C). The following relationship observed between applied current and potential is called the Tafel equation

$$i_{app} = i_{corr}\left[\exp\left(\frac{2.3(E - E_{corr})}{\beta_a}\right) - \exp\left(\frac{-2.3(E - E_{corr})}{\beta_c}\right)\right]$$

where E is applied potential, E_{corr} is open-circuit potential (or equilibrium potential), i_{app} is applied current density based on the electrode surface area, i_{corr} is corrosion current density, and β_a and β_c are anodic and cathodic Tafel coefficients related to the slopes of the polarization curves in the anodic and cathodic regimes, respectively.

From the obtained corrosion current, the corrosion rate is determined from the following equation

$$\text{Corrosion rate}(mm/yr) = \frac{i_{corr} \times E.W. \times 10}{\rho \times F}$$

where i_{corr} is corrosion current density (A/cm^2), E.W. is equivalent weight (g/equivalent) of the metal specimen, ρ is density (g/cm^3) of specimen, and F is Faraday's constant (96500 C/g-equivalent).

2.5 X-ray Diffraction

X-ray diffraction (XRD) provides a unique and practical means for obtaining mineralogical information on the corrosion product. Such information includes crystal size and disorder, structural parameters (unit cell edge length), composition, number of phases, and the percentage of phases that are present in a material [13]. Some other applications involve precise measurements of lattice constants and residual strains, and refinement of atomic coordinates [14].

When a monochromatic x-ray beam passes through a crystalline material, x-rays are diffracted at various angles with respect to the incident beam. The electromagnetic waves of incident x-rays are scattered by atomic planes in material, which results in the destructive and constructive interference of scattered waves. The relationship between the wavelength (λ) of x-ray beam, the angle (2θ) of diffraction, and the distance (d) between each set of atomic planes ($h\ k\ l$) of the crystal lattice is described by Bragg's equation:

$$n\lambda = 2d_{hkl} \sin\theta$$

where n is an integer. This method is useful for identification of corrosion products formed on the surface of metal and its purity.

2.6 X-ray Fluorescence (XRF)

X-ray fluorescence is a simple and generally nondestructive method for qualitative and quantitative analysis of elemental composition in a wide range of materials. This method is very useful because of the ease in sample preparation and because of its ability to detect and analyze elements with an atomic number greater than elements as light as boron under certain circumstances [14].

XRF is based on the photoelectric effect. When an atom is irradiated with highly energetic photons, an electron from one of the inner shells may be ejected. As an electron from the outer shell fills the vacancy, a photon with energy characteristic of the atom is released. This radiation is called fluorescent radiation, and each element has its own set of characteristic emission or x-ray fluorescence lines. The intensity and the energy of these lines are measured using a spectrometer. Most recent spectrometers use microprocessors and/or personal computers to automate data collection and to present the results of elemental analysis in an easily understandable format. Also, computer programs enable semiquantitative analysis without the use of internal standards. In analysis with XRF, the limitations are the decrease in the sensitivity for elements lighter than oxygen. The standards of similar composition and morphology are required for accurate quantitative analysis.

2.7 Scanning Electron Microscopy/Energy Dispersive X-ray Spectroscopy

Scanning electron microscopy (SEM) is used to obtain an electron image of the morphologic and topographic information of a material surface. For an electron microscopic image, the surface of a material is scanned in a raster pattern with a finely focused beam of electrons. When the energetic beam of electrons scans the surface,

signals including secondary, back-scattered electrons are produced from the surface. The secondary electron signal is usually used to modulate the brightness of the cathode ray display screen, thereby forming the image. The secondary electron emission is determined to a large extent by the surface topography. When the image is formed from the back-scattered electron signal, the contrast is determined largely by compositional differences in the sample surface rather than topographic characteristics. The intensity of the signal is proportional to the number of electrons emitted from each scanned location on the surface. The difference in signal intensity from different locations allows an image of the surface to be formed.

Environmental scanning electron microscopy (ESEM) is a useful method in obtaining the electron image of conductive material as well as nonconductive material without coating the sample. This method allows examination of a sample under small pressures as opposed to vacuum. When electrons emitted from the sample travel through the gaseous environment, collisions occur between an electron and the gas and result in emission of more electrons and ionization of the gas molecules. This increase in the amount of electrons effectively amplifies the original secondary electron signal. The positively charged gas ions are attracted to the negatively charged sample resulting in sample charging [14]. ESEM is more suitable for the study of metal oxides produced through the corrosion process.

Energy dispersive x-ray (EDX) analysis is used to obtain the quantitative information about the elemental composition on the local surface of the material. In addition, the elemental distribution of the surface can be mapped. This analysis is used in conjunction with ESEM imaging, thereby allowing analysis to be performed directly on areas under electron beam observation [15].

2.8 X-ray Absorption Fine Structure Spectroscopy

X-ray absorption fine structure spectroscopy (XAFS) provides the most reliable means for obtaining the local structural environment of a material. XAFS does not require long range order and is equally applicable to amorphous materials in its ability to probe the environment of an element in the sample by selecting and tuning to the edge energy [16].

The simplest XAFS experiments may be conducted in transmission mode as shown in Figure 2.1. The sample is mounted on the stage and the incident and transmitted x-rays are detected with ion chamber as the energy is varied over the absorption edge. The spectra include the near edge and fine structure over the edge; both providing information on the coordination environment with respect to the types of atoms surrounding the probe species, bond distances, and the oxidation state. XAFS refers to the sinusoidal variation of the x-ray absorption coefficient as a function of x-ray photon energy occurring beyond each absorption edge of an element.

In the classical limit, the fine structure above the absorption edge can be viewed as interference between the photoelectron wave ejected from the target atom and waves scattered from its neighboring atoms. The Fourier transform of these spectral features

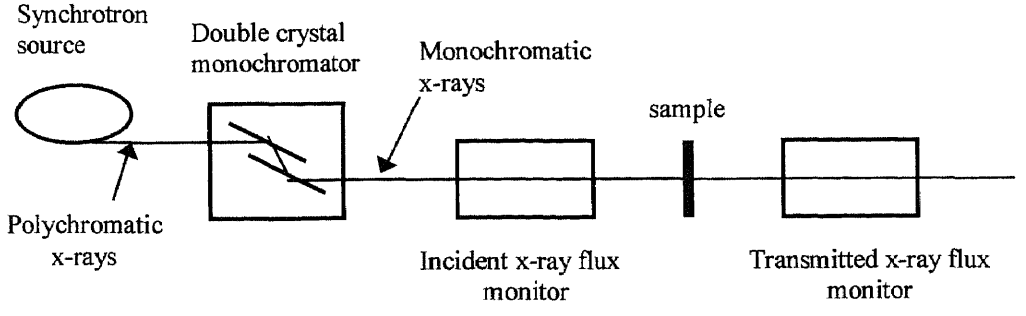

Figure 2.1 Schematic XAFS experiment in transmission mode

yields a qualitative representation of the radial distribution function. Structural parameters are determined by least-squares analysis providing the distance, number, type of neighboring atoms, and an estimate of the disorder affecting the interatomic distance [16].

CHAPTER 3

MATERIAL AND EXPERIMENTAL METHODS

Immersion corrosion tests in concentrated HCl solution were conducted for the study of steel corrosion. The characterization methods used in these experiments including mass loss measurement, x-ray diffraction, x-ray fluorescence, scanning electron microscopy/energy dispersive x-ray spectroscopy, and x-ray absorption spectroscopy are presented in this chapter.

3.1 Material

For this corrosion study, the steel substrates used, gun-barrel steel, were obtained from the U.S. Army. The mechanically polished specimens were rectangular coupons with an average dimension of 0.06 cm × 2.06 cm × 2.06 cm. The specific thickness, planar surface area, and weight of each specimen are listed in Table 3.1. The density of the steel substrate was measured as 7.62 g/cm^3.

3.2 Test Procedure

The preparation of specimen and immersion corrosion test was based on American Society for Testing and Materials (ASTM) procedures (G 1-90 and G 31-72) [16]. The steel substrate specimens were initially cleaned in acetone solution to remove grease from the surface and then weighed. The concentrated (37.8% (w/w) or 12.3 M) hydrochloric acid was used as corrosive medium for the gun-barrel specimens as it is the most corrosive acid on steel (Table 3.2) [18]. Acid aggressiveness follows the general trend of HCl> H_2SO_4 >H_3PO_4>HNO_3.

Table 3.1 Thickness, size, and weight of each steel substrate used in the corrosion test

Sample name	Size (cm)	Thickness (mm)	Weight (g)
Steel substrate as control	2.06 x 2.05	0.65	2.09200
1st experiment :			
1 HR	2.06 x 2.05	0.61	1.97046
8 HR	2.06 x 2.04	0.66	2.10410
16 HR	2.05 x 2.04	0.66	2.11689
24 HR	2.06 x 2.05	0.65	2.09412
41 HR	2.06 x 2.05	0.64	2.05650
2nd experiment :			
10 min	2.06 x 2.05	0.49	1.56485
20 min	2.06 x 2.06	0.48	1.55306
40 min	2.06 x 2.07	0.48	1.56015
1 HR	2.06 x 2.06	0.50	1.60750
3rd experiment :			
1 HR	2.06 x 2.04	0.60	1.92211
6 HR	2.06 x 2.05	0.50	1.62893
16 HR	2.06 x 2.05	0.49	1.58247
24 HR	2.06 x 2.05	0.49	1.57527

Table 3.2 Corrosion rates of stainless steel in acid media [17].

Acid	Concentration (%)	Temperature (°C)	Corrosion rate (mm/yr)	AISI type
HCl	37	24	169.2	302
H_2SO_4	60	43	5.08	316
H_3PO_4	85	124	2.79	316
HNO_3	90	Boiling point	1.27	316
CH_3COOH	10	Boiling point	1.75	302

In the immersion corrosion test, each steel substrate specimen was immersed in 300 ml of HCl solution. As shown in Figure 3.1, the scheme of the apparatus, the specimen was located approximately 4 cm from the bottom of the beaker. Agitation was maintained with the Reynolds number between 10,000 and 16,000 indicative of a turbulent regime

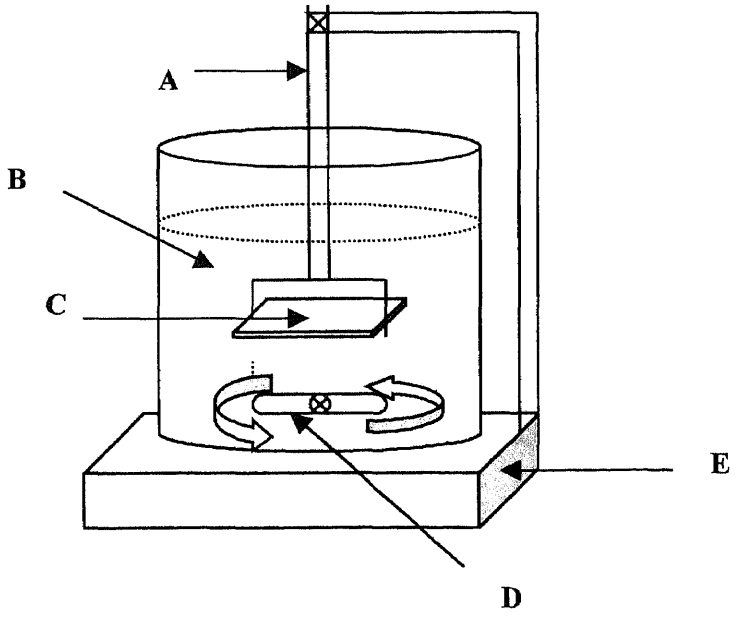

Figure 3.1 Scheme of apparatus for immersion corrosion test.

A=sample holder, B=HCl solution, C=steel substrate, D=magnetic stiring bar, and E=stirrer

[19]. For the calculation of the Reynolds number in an unbaffled tank, the length of the stirrer was used as the reference length and the stirrer length times the rate of stirrer rotation per unit time was employed as the reference velocity.

The corrosion test in an open system was conducted at room temperature (24 ± 1°C) with exposure times ranging from 10 minutes to 41 hours. After each test, the corroded steel substrate was dried and analyzed with x-ray diffraction (XRD), x-ray fluorescence (XRF), scanning electron microscopy (SEM)/energy dispersive x-ray (EDX), and x-ray absorption fine structure (XAFS). In order to measure the corrosion rate by the mass loss measurement, the corrosion product was removed mechanically from the surface of each specimen using a brush, and the weight was recorded.

3.3 Methods of Analysis

3.3.1 Mass Loss Measurement

Corrosion rates were calculated by measuring weight before and after the corrosion test over various exposure times: 1, 8, 16, 24, and 41 hours in the first experiment; 10, 20, 40, and 60 minutes in the second experiment; and 1, 6, 16, and 24 hours in the third experiment. The corrosion product was mechanically removed from the surface of corroded steel specimen using a brush with fiber bristles. Corrosion rate was expressed as thickness loss (mm) per time (year). The following equation was used for the corrosion rate calculation:

$$mm/yr = 87.6\frac{M}{\rho \times A \times t}$$

where M is mass loss of metal (mg), ρ is density of metal sample (g/cm^3), A is exposed area of metal sample (cm^2), and t is exposure time (hr).

Each solution after the corrosion test (for the first experiment) was filtered through a membrane filter with the pore size of 0.45 μm, and the concentration of iron in the filtrate was measured with a Perkin-Elmer AA spectrometer.

3.3.2 X-ray Diffraction and X-ray Fluorescence

X-ray diffraction patterns of the steel substrate and its corrosion products were measured using a Philips X'Pert-MPD XRD system with PC-APD software. X-rays were generated with a Cu $K\alpha$ x-ray source (λ=1.54056Å) operating at 40 mA and 45 kV. The data were collected over 2θ range from 5° to 110°. Because no commercial standard material for the iron oxide including β-FeOOH (Akaganeite) was available for this XRD study, the akaganeite was synthesized according to Schwertmann and Cornell's method [13]. XRD patterns were compared with iron oxide reference patterns from the powder diffraction file (PDF) established by the Joint Committee on Powder Diffraction Standards (JCPDS) to identify the specific iron oxide compound from the corrosion products and to obtain the structural information for XAFS analysis.

The composition of the steel substrate and its corroded specimens was evaluated using a Philips PW2400 XRF system with SemiQ software. Because no standard materials for steel and iron oxide were available, semi-quantitative analysis was conducted instead of quantitative analysis.

3.3.3 Scanning Electron Microscopy /Energy Dispersive X-Ray Spectroscopy

The morphological information of the corroded steel surface was obtained using LEO 982 FE-SEM operated at the working distance of 15 mm and an accelerating voltage of

15 kV. The elemental composition on the corroded surface was examined using EDX with Oxford ISIS EDS System at the same operating condition as the SEM. The magnification used in SEM was 1000×, and in the case of EDX a minimum magnification of 50× was selected to scan the larger area of the corroded surface.

3.3.4 Extended X-ray Absorption Fine Structure Spectroscopy

XAS data acquisition for the steel substrate and corroded steel specimens was performed on beamline X-11A at the National Synchrotron Light Source (NSLS), Brookhaven National Laboratory. The storage ring operates at 2.58 GeV with a typical current of 100 mA. The monochromatic radiation used in this study was acquired with two parallel Si (111) crystals detuned 20% from the fully tuned incident (I_o) radiation. The slit size was 1 mm (vertical) by 10 mm (horizontal). Fluorescence mode for the Fe *K*-edge (7.112 KeV) as shown in Figure 3.2 was applied for the steel and its corroded specimens. X-ray intensities were measured at room temperature using a Stern-Heald type detector filled with Ar gas. A manganese filter (Z-1) for the Fe *K*-edge was used to minimize the

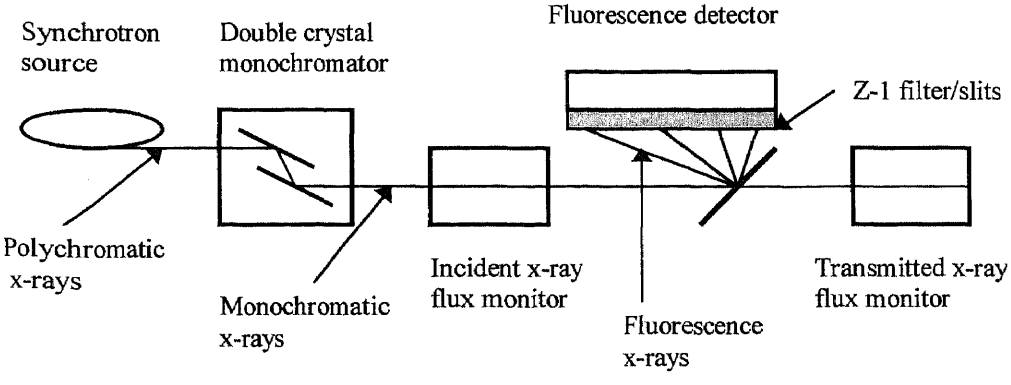

Figure 3.2 Schematic XAFS experiment in fluorescence mode

scattered background. Samples were positioned 45° to the incident radiation beam (I_o). Soller-slits were positioned between the sample and detector to reject elastic scatter. The XAFS data were collected over the range of 6900 to 8200 eV.

The XAFS data analyses were performed using standard procedures [20] and the program WinXAS 1.0 and Feff 7 for computation of the model scattering amplitude and phases.

CHAPTER 4

RESULTS AND DISCUSSION

In this section, results from corrosion studies are presented and include data from the weight loss measurements, ESEM\EDX, XRD, XRF, and XAFS.

4.1. Corrosion Rate

Based on weight loss data from steel exposed to 37.8% hydrochloric acid, Figures 4.1 and 4.2 illustrate corrosion rates (mm/yr) over a period of 10 minutes to 1 hour and 1 hour to 41 hours, respectively. The plot of weight loss per unit area of the corroded steel specimen versus exposure time is shown in Figures 4.3 and 4.4. In these figures, the error bar (less than 0.1%) is within the size of the symbols.

As indicated in Figure 4.1, weight loss of steel specimen during 10 minute-exposure period was too small to detect. However, corrosion rates over the exposure time up to 1 hour appeared to increase linearly. Between exposure times of 1 and 8 hours (the first experiment), the samples revealed the greatest weight loss per unit area. For greater than 8 hours, the weight loss per unit area gradually decreased. Corrosion measured as weight loss per unit area of steel tends to proceed exponentially as a function of exposure time (Figure 4.2). Rates were the greatest in the initial stages of corrosion (up to 8hr), subsequently, they decreased greatly. In the third experiment, the steel specimens exposed for 16 and 24 hours were completely dissolved in the solution.

Corrosion rates reported in literature [18] are often based on steady state conditions. Initially, the uncorroded steel surface oxidizes rapidly in hydrochloric acid at room temperature, and the chemical reactivity diminishes as reaction time increases. The

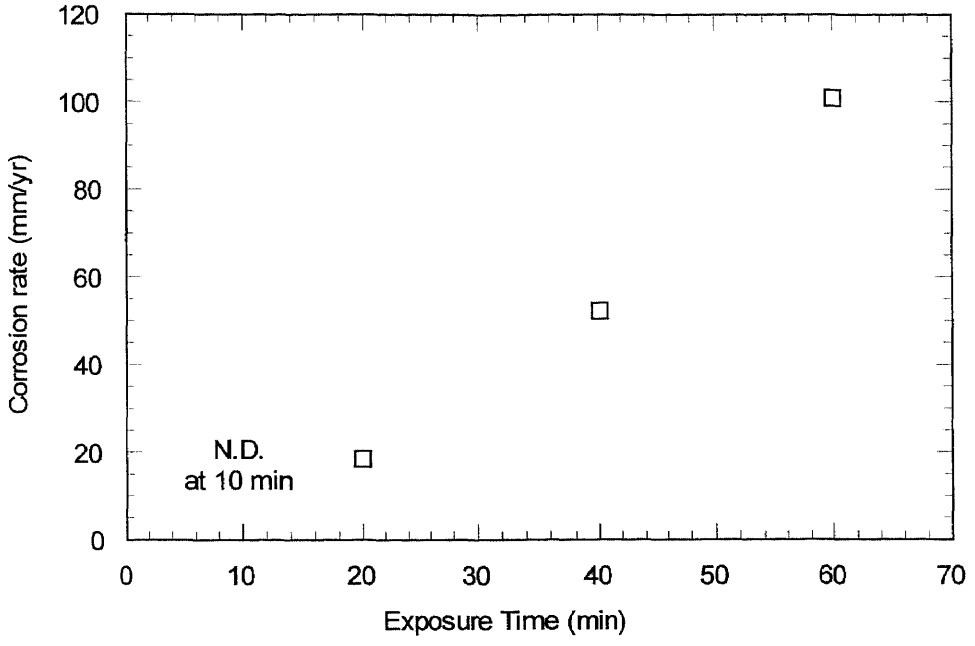

Figure 4.1 Corrosion rate of corroded steel specimen at room temperature from the second experiment

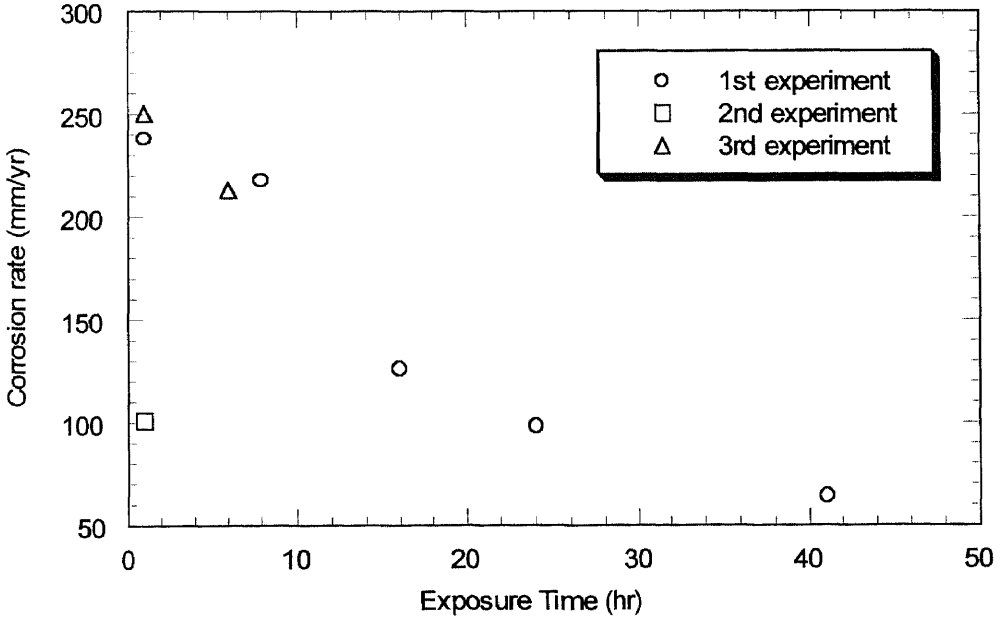

Figure 4.2 Corrosion rate of corroded steel specimens at room temperature from the three experiments

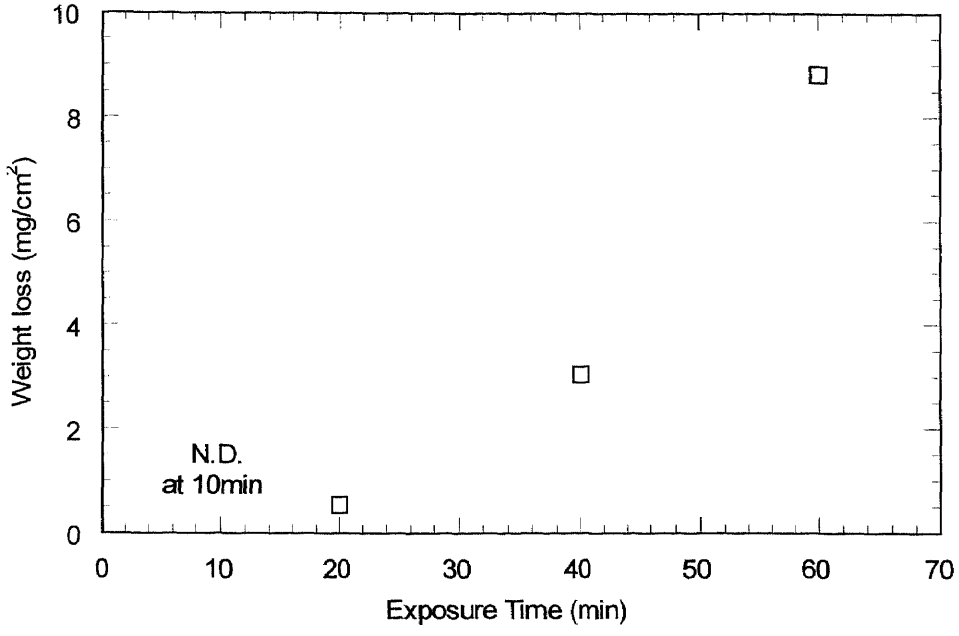

Figure 4.3 Weight loss per unit area of corroded steel specimens from the second experiment

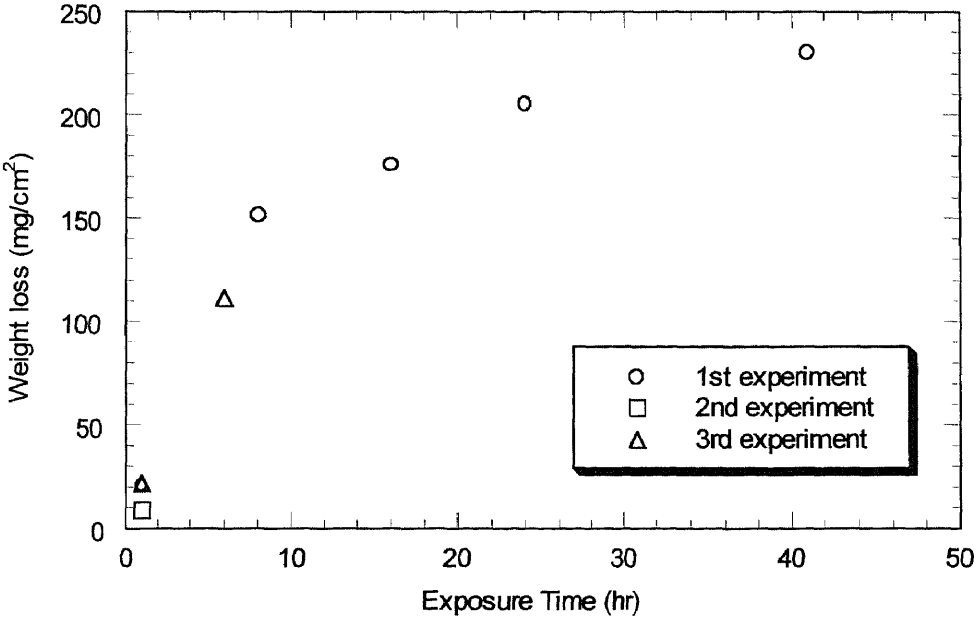

Figure 4.4 Weight loss per unit area of corroded steel specimens from the three experiments

decrease in corrosion rates can be attributed to formation of the oxide corrosion product that inhibits transport of the oxidizing agent (O_2) to the steel surface.

The corrosion rate during 1 hour-exposure time as seen in Figure 4.2 varies from 101 to 250 mm/yr. The differences between these three experimental studies included the following :

- The N_{Re} varied between experiments: in the first experiment, it was 11,000 to 13,700; in the second experiment, it was 11,000 to 13,700; and in the third experiment, it was 13,700 to 16,000. All the regimes are turbulent (N_{Re}>10,000) [19], therefore, the corrosion results can not be explained from the hydraulic regime.
- Sample configuration for each experiment was slightly different with respect to location in the batch reactor. No baffles were used and therefore a vortex is formed. Depending on the sample depth, the specimen will receive a different scouring force due to the vortex.
- Sample area had a small variance due to different thicknesses, which averaged 0.64 mm in the first experiment, 0.49 mm in the second experiment, and 0.52 mm in the third experiment. However, these effects would result in much smaller differences in corrosion rates than what was observed.
- One other potential explanation may be that samples from the first and third experiments had more scratches or defects expediting corrosion as compared to the second experiment.

As the steel substrate corrodes, the decrease in corrosion rate is also due to the passivity of the iron oxide film. Most metal oxides are less reactive to corrosive media than the steel. Moreover, the crystallization of iron oxide film decreases the corrosion

rate, as the crystalline oxide film can decrease mass transfer of the oxidizing agent to a corrosion site. In this study, a batch reactor was used and therefore the concentration gradient was not a driving force in the experiment. However, in a constant flow environment such as a gun-barrel or water distribution system, a concentration gradient may result in an increase in corrosion due to the oxide having a greater solubility than the steel.

Table 4.1 shows that the amount of dissolved iron in solution as a function of time for the first experiment using the AA spectrometer. The percent dissolution is the ratio of the dissolved iron to the total iron measured from weight loss, which indicates that a relatively small portion of iron from the weight loss measurement consisted of iron oxide. As shown in Figure 4.5, the difference in the amount of iron between measured and calculated values indicates the portion of iron, which exists as the corrosion product.

Table 4.1 The amount of iron dissolved in solution from the first experiment (AA anaylsis)

Exposure time (hour)	Amount of Fe ions measured by AA (g)	Amount of Fe from weight loss measurement (g)	Dissolution (%)
1	0.12100	0.16473	73.5
8	1.08750	1.19543	91.0
16	1.15125	1.38959	82.8
24	1.32750	1.63364	81.3
41	1.42500	1.82974	77.9

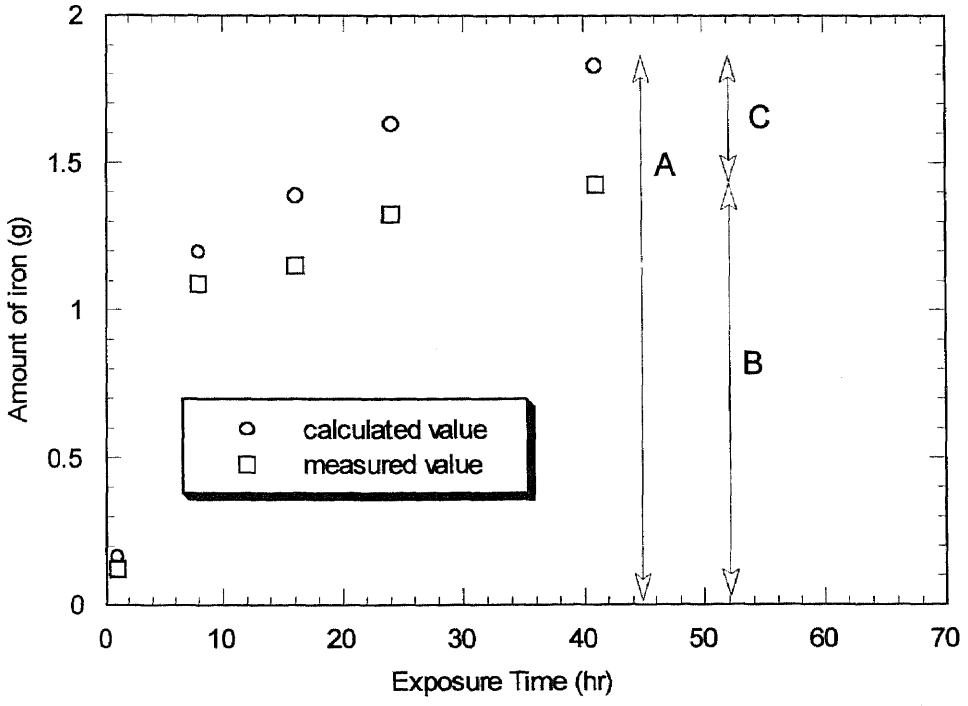

Figure 4.5 The concentration of iron dissolved in solution from the first experiment (A is total amount of iron from weight loss measurement, B is dissolved amount of iron from AA analysis, and C is the amount of iron existing in corrosion product as iron oxide)

4.2 Scanning Electron Microscopy/Energy Dispersive X-ray Spectroscopy Analysis

SEM examination

The morphological information for the steel surface and its corroded specimens was obtained using SEM as shown in Figure 4.6. The SEM of Image A revealed that the steel substrate prior to corrosion was scratched parallel to the polished direction and showed some defects.

Images B to F show the morphological change of the corroded steel substrate as a function of exposure time from 1 to 41 hours. At the initial stages of corrosion (1 hour),

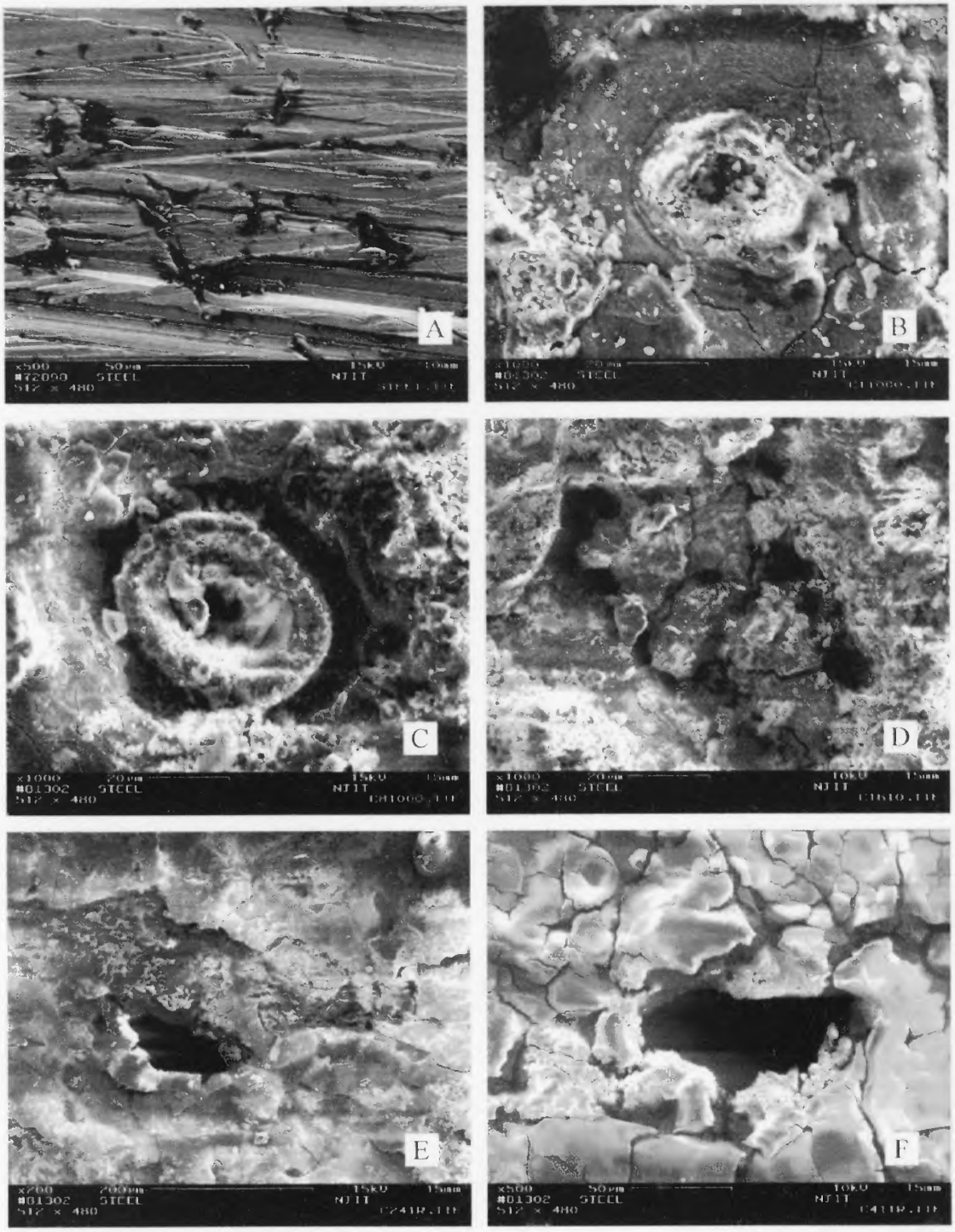

Figure 4.6 SEM images of the steel substrate surface and its corroded specimens from 37.8% HCl solution as a function of time. A: Steel Substrate (500×); B: 1hr corroded steel (1000×); C: 8hr corroded steel (1000×); D: 16hr corroded steel (1000×); E: 24hr corroded steel (200×); and F: 41hr corroded steel(500×).

Image B reveals that the surface starts pitting resulting in small oxide particles constituting the corrosion product. The dominant oxide formed is β-FeOOH (Akganeite), and will be discussed in Section 4.4. The surface of corroded steel substrate at an 8 hour-exposure time appears to be severely attacked as shown in Image C compared to the morphology of the 1 hour specimen. Image D shows that the crystallized corrosion products appear as agglomerates of the oxide particles. Impressive features (Images E and F) are seen on the surfaces at 24 and 41 hour-exposure times. The two corroded specimens are most severely attacked and hence the steel has been penetrated to some degree. In the case of the 41 hour specimen, corrosion products appear to be agglomerated throughout the point of penetration.

EDX quantitative analysis

The elemental composition of the steel surface and corroded specimens was examined by EDX. Data from quantitative analysis for the specimens are listed in Table 4.2, and based on weight percent. The steel substrate surface is composed of Fe and C with minor amounts of Ni, Cr, and Mn (Figure 4.7). The steel substrate was expected to be similar to AISI 4340 steel based on communication with Dr. Marek Sosnowski [21]. EDX results indicate that this gun-barrel steel appears to have more carbon than either carbon steel or stainless steel, which generally contains carbon less than 1% [22]. If the chamber was contaminated, then all the specimens would have shown carbon. This was not observed.

Figure 4.8 shows EDX spectra for the surface of steel specimens corroded in 37.8% HCl solution at room temperature as a function of exposure time. As seen in Table 4.2, oxygen is present in the range of 42% to 45%. The presence of oxygen indicates that an iron oxide film has precipitated. Chloride is the third major constituent in each of the

Table 4.2 EDX quantitative analysis data (w/w %)

Element	Steel Substrate	Corroded Steel Substrate				
		1HR	8HR	16HR	24HR	41HR
Fe	84.19	50.48	52.18	51.87	50.16	51.59
O	-	45.18	43.75	42.02	45.20	44.60
C	10.75	–	–	–	–	–
Ni	1.98	1.65	1.05	1.56	0.29	1.75
Cr	0.74	0.48	0.51	0.51	0.23	0.32
Mn	0.60	0.77	0.20	0.36	0.37	0.62
Al	0.55	–	–	–	–	–
Cu	0.49	–	–	–	–	–
Si	0.28	–	–	–	–	–
S	0.20	–	–	–	–	–
P	0.06	–	–	–	–	–
Cl	0.05	1.45	2.31	3.68	3.76	1.12

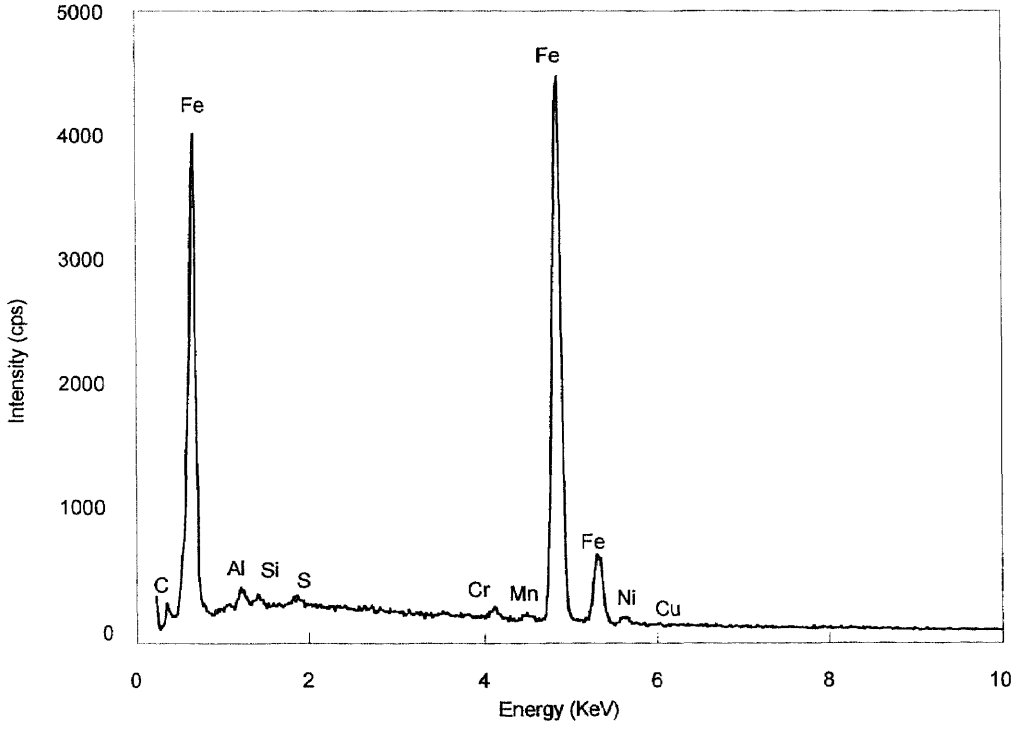

Figure 4.7 EDX spectrum of the steel substrate

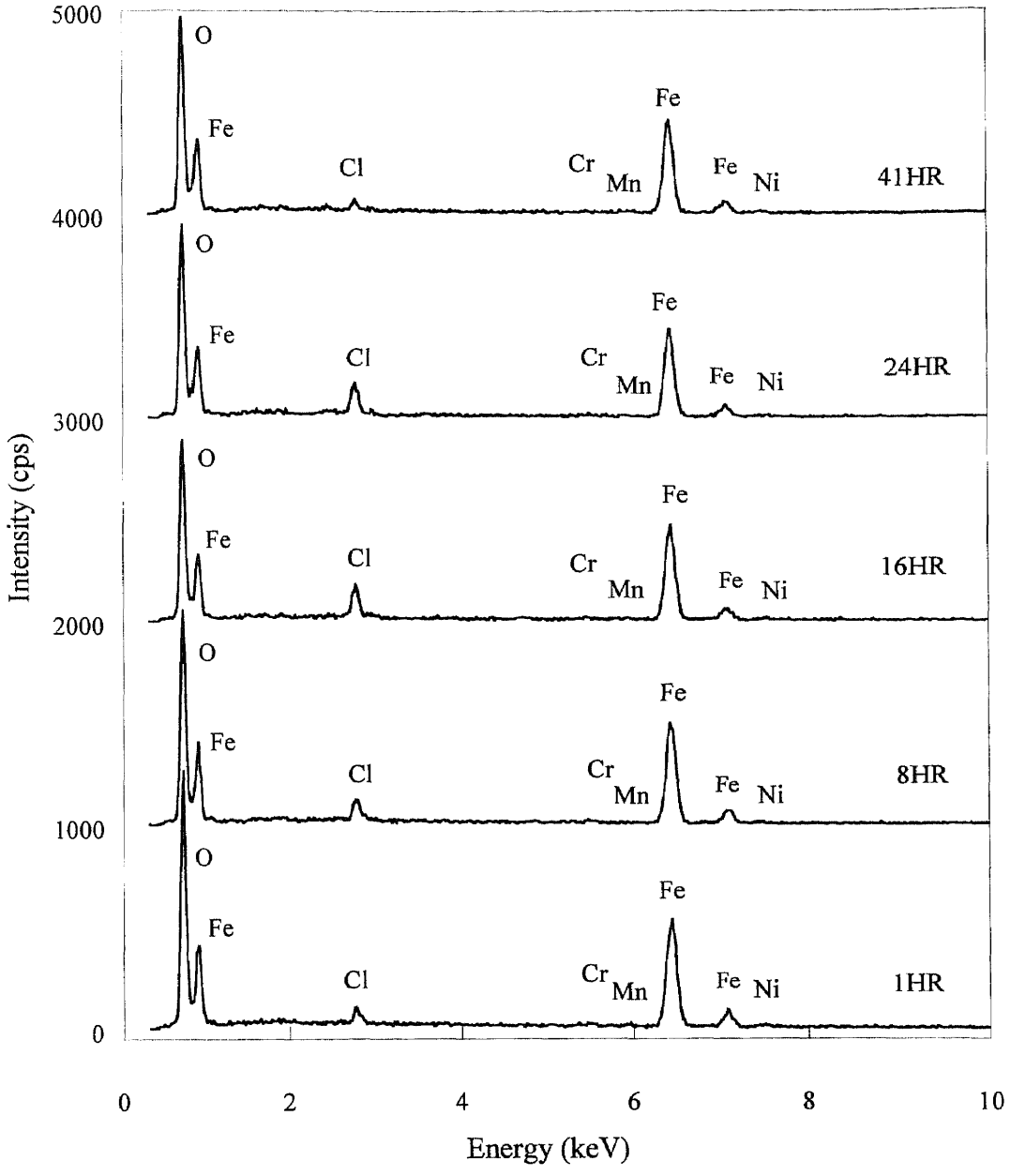

Figure 4.8 EDX spectrum of the corrosion product for corroded steel specimens

corroded steel specimens ranging between 1.12% and 3.68%. Mass transfer of chloride ions through the oxide film results in an increase in the chloride concentration. Furthermore, Post and Buchwald [20] found that the tunnel sites in the crystal structure of akaganeite are partially occupied by chloride.

The EDX patterns for the corroded specimens are similar to each other in the peak position and intensity for each spectrum. This similarity indicates that the corrosion products appear to have comparable composition, if not identical, even though the composition ratio of each element varies slightly as a function of exposure time. Overall, exposure time had little effect on the corrosion product composition.

4.3 X-ray Fluorescence Analysis

The bulk compositional information for steel substrate and its corroded specimens was obtained semi-quantitatively using XRF with SemiQ software. The Semi-quantitative data are listed in Table 4.3. Although XRF does not detect carbon and oxygen, the sensitivity of XRF provides greater accuracy than EDX. In addition, x-rays are used to probe the specimen with XRF, while electrons are employed with EDX; therefore, the depth of study is extended from 0.5 μm with EDX to 50 μm with XRF.

In the case of the steel substrate, the elements given in Table 4.3 were detected and the weight percent of each element is consistent with data from the EDX analysis. In addition, data from the corroded steel specimens show that the composition is similar to results from the EDX analysis.

Table 4.3 Semi-quantitative analysis of XRF for the steel substrate and corroded steel specimens (w/w %)

Element	Steel Substrate	Corroded Steel substrate				
		1HR	8HR	16HR	24HR	41HR
Fe	94.11	92.45	89.73	88.20	86.15	88.48
Ni	2.51	2.48	2.45	2.43	2.07	2.43
Cr	1.00	1.07	1.02	1.01	1.10	1.43
Mn	0.58	0.63	0.60	0.61	0.51	0.60
Al	0.93	–	–	–	–	–
Cu	0.10	0.11	0.14	0.14	0.12	0.16
Si	0.08	0.04	0.05	0.03	0.04	0.04
S	0.02	–	–	–	–	–
P	0.01	–	–	–	–	–
Cl	0.06	2.33	5.17	6.48	7.52	1.81
Mo	0.50	0.72	0.75	0.97	1.91	4.90
V	0.10	0.13	0.15	0.17	0.49	0.06

4.4 X-ray Diffraction Analysis

X-ray diffraction patterns for the steel substrate and the corroded steel specimens over the exposure time of 10 and 20 minutes are shown in Figure 4.9. The steel substrate showed reflections corresponding to a 2θ of 44.76° (110), 65.05° (200), 82.29° (211), and 98.66° (220) with the (110) orientation exhibiting the greatest diffraction intensity. The XRD pattern of steel substrate appears to match alpha iron well, which has

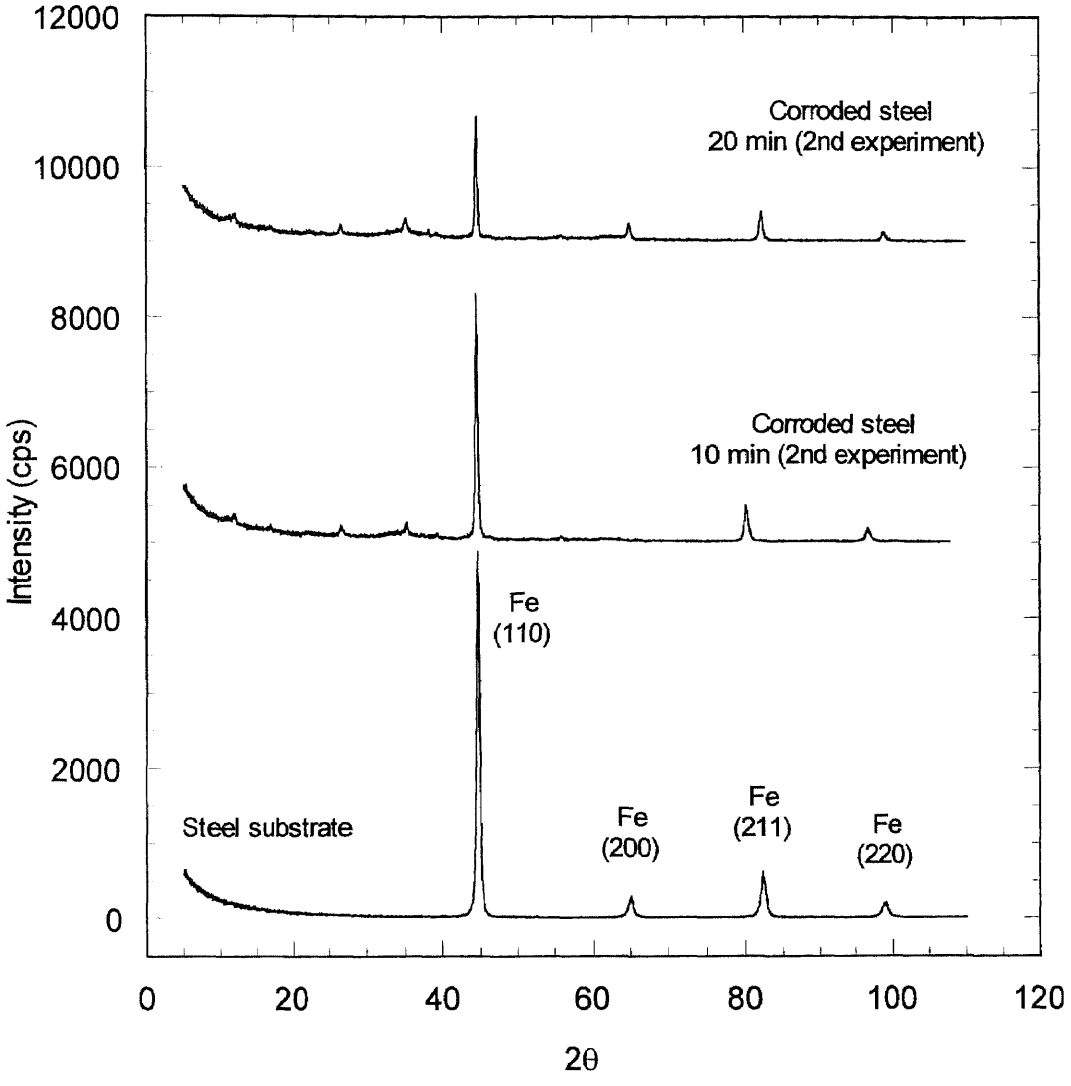

Figure 4.9 XRD patterns for the steel substrate and the corroded steel specimens from the second experiment with 10 and 20 minute-exposure time

a body centered cubic (bcc) structure. No preferred orientation was observed. As listed in Table 4.4 the distance between the central atom and neighboring atoms was calculated based on the bcc structure and the *hkl* reflections. As indicated in Figure 4.9, XRD patterns of the corroded specimens over the exposure time of 10 and 20 minutes appear to be similar to that of the steel substrate. However, the peak intensity indicating Fe (110) decreased as the exposure time increased up to 20 minutes. Therefore, formation of a very thin oxide film may have suppressed the X-ray beam diffracted from the steel substrate. Also, the presence of peaks in 2θ less than 40° suggests oxide precipitation.

Figures 4.10 and 4.11 show the XRD patterns for the synthesized akaganeite standard and the corroded steel surface as a function of exposure time. Some peaks indicate reflections corresponding to that of the steel substrate underlying the corrosion product. XRD peaks for 1 hour and 8 hours in the first experiment show similar patterns indicative of β-FeOOH (akaganeite) based on crystal structure study of akaganeite crystal [23]. The mineral akaganeite is known as the dominant mineral existing when Cl^- or F^- is present [24]. As exposure time increased, a surface structure constituting akaganeite was evident over a period of 1 hour to 24 hours.

Table 4.4 2θ widths of bcc reflections for the steel substrate

d-value (°2θ)	*hkl* reflection	Peak width(°2θ) at half height	R(Å)
2.0268	(110)	0.455	2.8663
1.4332	(200)	0.717	2.8664
1.1702	(211)	0.837	2.8664
1.0134	(220)	0.926	2.9172

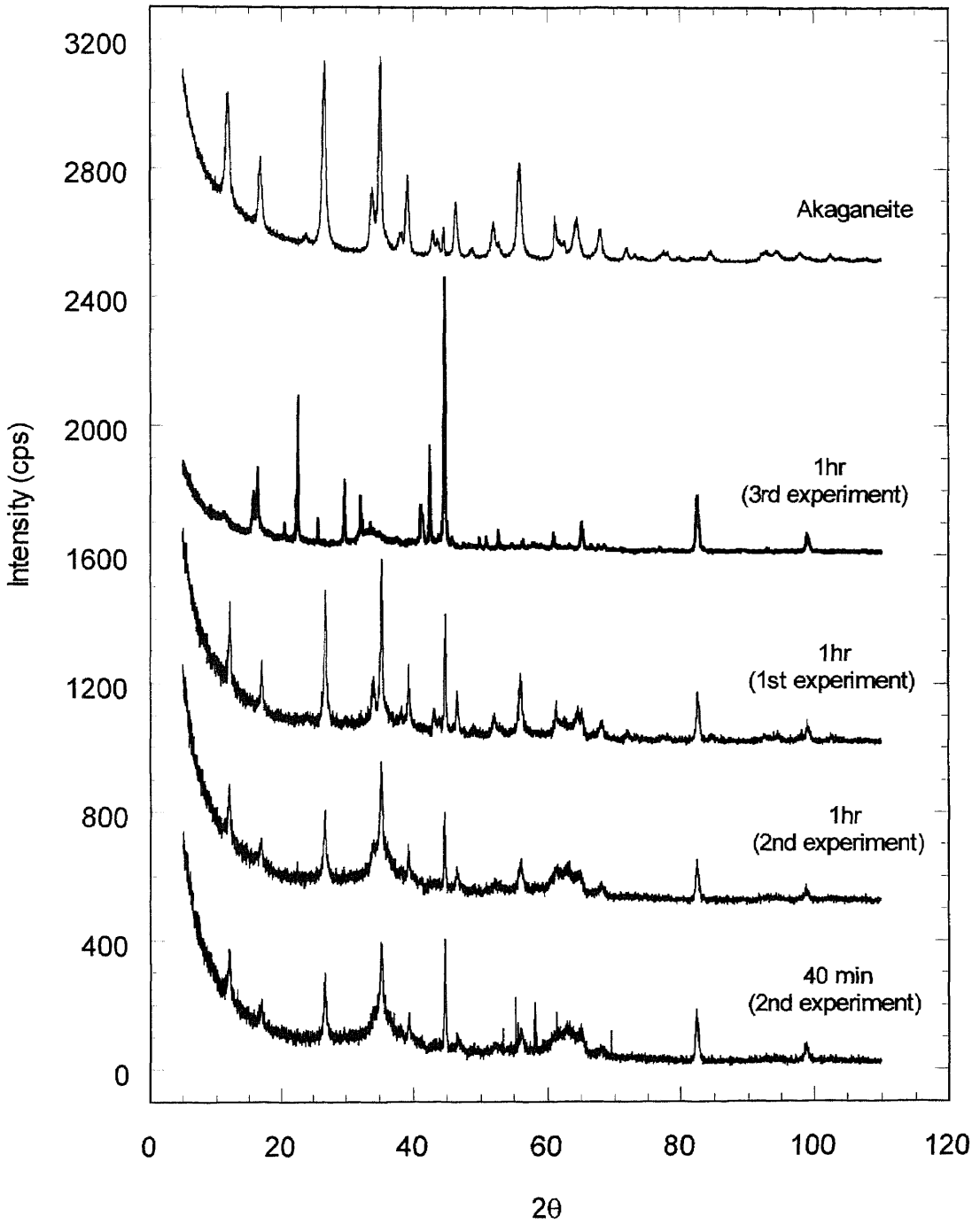

Figure 4.10 XRD patterns of synthesized akaganeite standard and corroded steel specimens from the three experiment

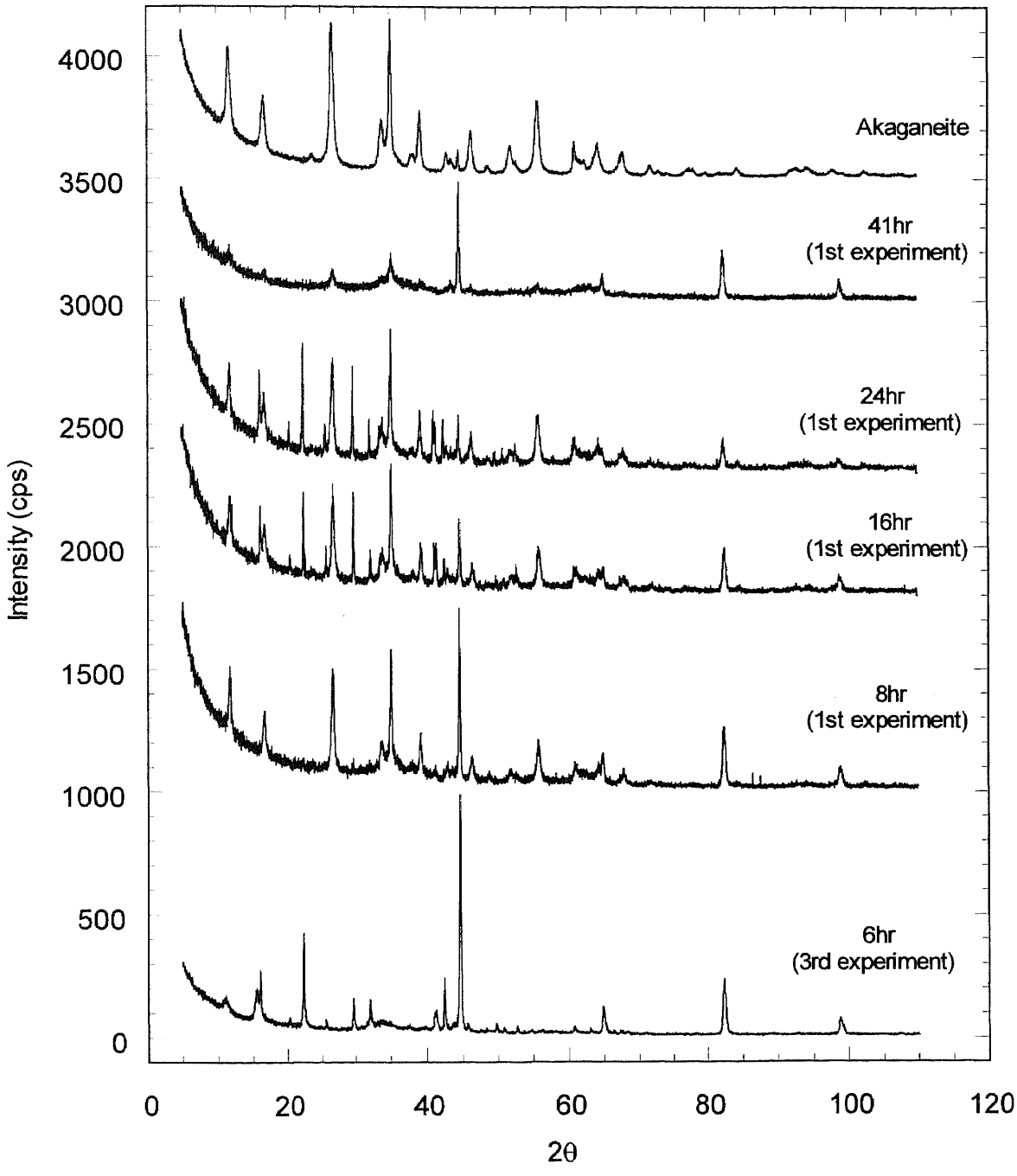

Figure 4.11 XRD patterns of synthesized akaganeite standrad and corroded steel specimens from the first and third experiment

However, at 16 hours and 24 hours, additional peaks not seen in other samples appear to indicate the presence of other oxide compounds. Also, the background suggests an amorphous oxide is also present. The XRD of the 41 hours corroded specimen revealed some akaganeite, but the intensity of these peaks was relatively low compared to the intensity of the iron.

The difference in oxide and steel intensities between experiments may be explained by the varying sample location where some specimens received a greater scouring force than others during a corrosion test. As a result, more of the loosely held oxide may have been removed from the surface of the steel substrate. Another explanation for the differences, particularly for the 1 hour duplicates, may be that samples from the first and second experiments were stored in the dessicator for at least one month prior to XRD analysis. During this time, oxide formation from further corrosion may have occurred. Therefore, employment of an advanced storage system such as a vacuum dessicator instead of a conventional dessicator would prevent further corrosion of the sample and hence reduce the variations in the results.

4.5 X-ray Absorption Fine Structure Analysis

Figure 4.12 shows data in $\chi(k)\ k^3$ versus photoelectron wave vector (k) for models of α-Fe and β-FeOOH. The data of these models were obtained by using Feff7 program. Data reduced to $\chi(k)\ k^3$ versus k for steel and corroded steel specimens are presented in Figure 4.13. The 8 and 24 hours corroded specimens show strong oscillations at low k, suggesting backscattering of the first neighbor – an oxygen shell. Weak oscillations indicating an oxygen shell as the first neighbor are observed at low k in 41 hours

corroded sample. However, because less oxide was present and more signal was detected from the Fe in the steel substrate, the spectra of $\chi(k)\ k^3$ versus k for 1 and 41 hrs corroded specimens show no significant difference from that of the steel substrate. These data are considered to result from the thin corrosion product film on the surface of 1 and 41 hrs specimens. The monochromatic x-ray beam therefore penetrates into the steel substrate below the corrosion product film, resulting in backscattering of iron atoms in the steel substrate. The envelope for the backscattering of iron atoms is observed at higher k.

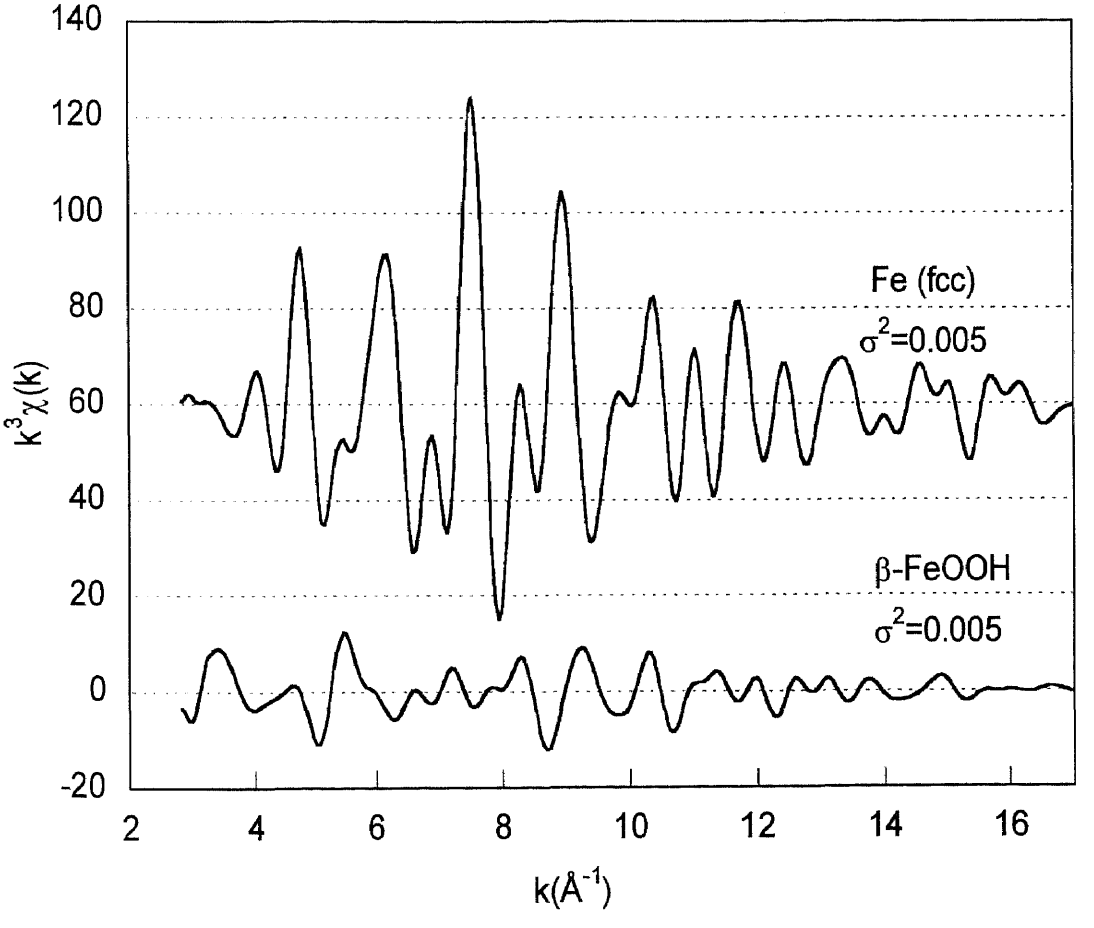

Figure 4.12. Data reduced to $\chi(k)\cdot k^3$ versus k for model of Fe(fcc) and β-FeOOH

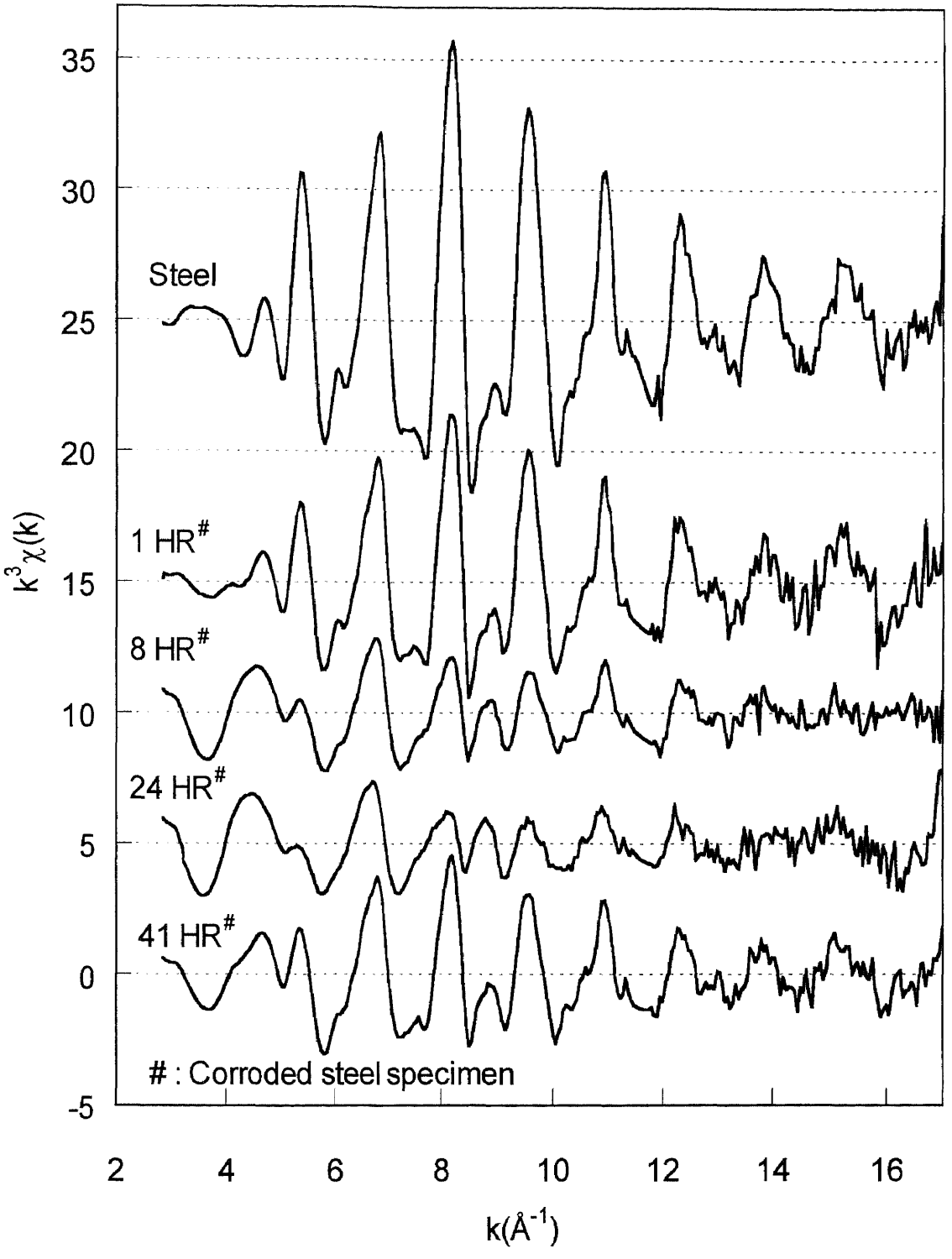

Figure 4.13. Data reduced to χ (k) k^3 versus k for the steel substrate and corroded steel specimens from the first experiment

Because iron exists in at least two oxidation states and has different coordination environments in steel and the oxide, the spectra are difficult to fit. One method that may be attempted in the future is to consider weighted fractions of the spectra.

CHAPTER 5

CONCLUSIONS

The purpose of this study was to evaluate the application of various characterization methods in assessing corrosion as a function of time. For this purpose, the immersion corrosion tests for the steel substrate in an aggressive environment were conducted as a control study over varying exposure times from 10 minutes to 41 hours. Subsequently, in the next phase of this research, tantalum corrosion will be evaluated under aggressive environments including elevated temperature and pressure. From this control study of the steel corrosion, the following can be concluded:

- The corrosion rate of steel substrate in 37.8% HCl solution at room temperature (24 ± 1 °C) initially increased up to 1 hour and then decreased as the exposure time increased up to 41 hours.
- XRD analysis indicated that the corrosion product of each sample consisted mainly of β-FeOOH (akaganeite) despite different exposure times. EDX results also revealed that the corrosion products for each specimen appeared to have identical surface composition. With XRF, the corroded samples were probed to a greater depth below the corrosion product. Nevertheless, similar bulk compositions were observed as compared to EDX. However, with XRF, carbon and oxygen are not detectable.
- SEM images on the corroded surfaces showed that the deeply scratched parts on steel substrate were severely attacked and were penetrated in corrosion tests as exposure time increased. However, polished steel surfaces showed uniform corrosion. Therefore, defects on the steel surface give rise to pitting corrosion.

- In EXAFS analysis, although the surface and bulk composition were equivalent, spectra for 1 and 41 hour-corroded specimens were different from those of 8 and 24 hours specimens. In the former specimens, an oxide film thinner than that of the others on the surface resulted in more signal from Fe atoms in the steel substrate than from the corrosion product. However, all the corroded specimens appear to have oxygen as the first neighbor. In order to obtain exact local structural information for each specimen, modeling of the data will continue in future studies.

This study provides a baseline for future corrosion research and an exploration of characterization methods for the corroded surface.

REFERENCES

1. P. Elliott, "Overcome the Challenge of Corrosion", *Chemical Engineering Progress*, pp. 33-42, May 1998

2. M. M. Kurtepov, "Corrosion of Chromium in Oxidizing Acid Solutions", *Theory and Practice of Chromium Electroplating*, pp. 142-144, 1965

3. *Fourth Annual Report on Carcinogens*, NTP 85-002, pp. 85, 1985

4. J. Chelius, "Use of Refractory Metals in Corrosive Environment Service", *Material Engineering Quart.*, pp. 57-59, August 1957

5. K. Anderson, K. Reichert, *et al.*, "Tantalum and Tantalum Compounds", *Ullmann's Encyclopedia of Industry Chemistry*, 5th completely revised edition, Vol. A26, editors; B. Elvers, S. Hawdkins, and W. Pussey, VCH, New York, 1995

6. M.G. Fontana and N.D. Greene, *Corrosion Engineering*, McGraw-Hill, 2nd ed., New York, 1978

7. U.R. Evans, *An Introduction to Metallic Corrosion*, 3rd ed., Edward Arnold, London, and American Society for Metals, Metals Park, OH, 1981

8. "Standard Practice for Preparing, Cleaning, and Evaluating Corrosion Test Specimens," G1, *Annual Book of ASTM Standard*, American Society for Testing Materials

9. L. L. Sheir, R. A. Jarman, and G. T. Barstein, *Corrosion; Corrosion Control*, 3rd ed., Butterworth and Heinemann Publisher, London, 1994

10. T. Shibata and Y. C. Zhu, "The Effect of temperature on the growth of anodic oxide film on titanium", *Corrosion Science*, Vol. 37, pp. 133-44, Jan., 1997

11. D.D. MacDonald and M.C.H. McKubre, *in Electrochemical Corrosion Testing, STP 727*, F. Mansfeld and U. Bertocci, Ed., American Society for Testing and Materials, pp. 110, 1981

12. *Application Note AC-1; Basics of Electrochemical Impedance Spectroscopy (EIS)*, EG & G Instruments, Inc., Princeton Applied Research, Princeton, New Jersey, 1989

13. U. Schwertmann and R.M. Cornell, *Iron Oxide in the Laboratory: Preparation and Characterization*, VCH Publishers, 1991

14. L.I. Maissel and R. Glang, *Handbook of Thin Film Technology*, McGraw Hill, Inc., New York, 1970

15. *Metal Handbook: V10 on Materials Characterization*, 9th ed., American Society for Metals, Metals Park, Ohio, 1986

16. B. K. Teo, *Extended X-ray Absorption Fine Structure Spectroscopy: Basic Principles and Data Analysis*, Chapters 2-6, Springer-Verlag, New York, 1986

17. "Standard Practice for Laboratory Immersion Corrosion Testing of Materials", G31, *Annual Book of ASTM Standard*, American Society for Testing Materials

18. J.F. Mason, Jr., *Metal Engineering Quarterly*; Section III: Corrosion Resistance and Protection, May, 1968

19. R. H. Perry, *Perry's Chemical Engineers' Handbook*, 6th edition, McGraw-Hill, Inc., New York, 1984

20. Bunker, B.; Sayers, D. *X-ray Absorption: Principles, Applications, Techniques of EXAFS, SEXAFS, and XAFS*, D.C. Koningsberger and R. Prins (editors) Wiley, New York, 1988.

21. M. Sosnowski (1998), Personal communication between Dr. M. Sosnowski and P. Shivaramkrishna during the course of the experiments, NJIT, Newark, NJ

22. D. Peckner and I. M. Bernstein, *Handbook of Stainless Steels*, McGraw-Hill, Inc., New York, 1977

23. J.E. Post and V.F. Buchwald, "Crystal Structure Refinement of Akaganeite", *American Mineralogist*, Vol. 76, pp.272-277, 1991

24. P. Keller, *Werkstoffe u. Korr.*, Vol. 20, pp. 102, 1969